Chinese Chemical Letters 34 (2023) 107087

Contents lists available at ScienceDirect

Chinese Chemical Letters

journal homepage: www.elsevier.com/locate/cclet

Talcum-doped composite separator with superior wettability and heatproof properties for high-rate lithium metal batteries

Mengqiu Yang[a], Yuanpeng Ji[a], Yunfa Dong[b], Botao Yuan[b], Liwei Dong[a], Yuanpeng Liu[b], Sue Hao[a,c], Chunhui Yang[a,c], Xiaoqiang Wu[d], Qingquan Kong[d], Jiecai Han[b], Weidong He[b,d,e,*]

[a] MIIT Key Laboratory of Critical Materials Technology for New Energy Conversion and Storage, School of Chemistry and Chemical Engineering, Harbin Institute of Technology, Harbin 150080, China
[b] National Key Laboratory of Science and Technology on Advanced Composites in Special Environments, and Center for Composite Materials and Structures, Harbin Institute of Technology, Harbin 150080, China
[c] State Key Laboratory of Urban Water Resource and Environment, Harbin Institute of Technology, Harbin 150080, China
[d] School of Mechanical Engineering, Chengdu University, Chengdu 610106, China
[e] Chongqing Research Institute, Harbin Institute of Technology, Chongqing 401151, China

ARTICLE INFO

Article history:
Received 26 November 2021
Revised 20 December 2021
Accepted 28 December 2021
Available online 4 January 2022

Keywords:
Lithium metal batteries
Composite separator
PVDF
Talcum
Wettability
Thermal stability

ABSTRACT

Separator is supposed to own outstanding thermal stability, superior wettability and electrolyte uptake, which is essential for developing high-rate and safe lithium metal batteries (LMBs). However, commercial polyolefin separators possess poor wettability and limited electrolyte uptake. For addressing this issue, we put forward a composite separator to implement above functions by doping layered-silicate (talcum) into polyvinylidene fluoride (PVDF). With significant improvement of electrolyte absorption benefiting from the strong adsorption energy values (-1.64 ~ -1.70 eV) between talcum and the electrolyte in lithium metal batteries, PVDF/Talcum (PVDF/TM) composite separator owns a small contact angle and superior electrolyte uptake. PVDF/TM composite separator with 10 wt% talcum (T-10) owns a tiny contact angle of 8°, while those of polypropylene (PP) and PVDF are 48° and 20° with commercial electrolyte. Moreover, the addition of thermotolerant talcum endows the T-10 composite separator with great thermostability, whose thermal shrinkage is only 5.39% at 150 °C for 0.5 h. The cell with $LiFeO_4$ cathode and the T-10 composite separator reaches 91.7 mAh/g in discharge capacity at 4.8 mA/cm^2 (10 C), far superior to that with pure PVDF separator (56.3 mAh/g) and PP (51.4 mAh/g).

Much effort has been made on the rechargeable lithium metal batteries (LMBs) for ever-increasing demands of novel portable electronics, long-range electric vehicles and solar/wind energy storage, owing to their high operating voltage, zero memory effect and long working lifetime [1–7]. However, the increasing demand for higher energy requires continuous optimization of key components in LMBs (cathode, anode, electrolyte and separator) [8,9]. As an inactive component, placed between cathode and anode, separator plays a vital role in capacity, cost-effectiveness, lifespan and safety of LMBs [10–18].

Polyolefin-based materials, for instance, polyethylene (PE) and polypropylene (PP), are used for commercial separators in LMBs due to their high mechanical strength and low cost [19–21]. However, the unsatisfactory thermal stability and wettability limit their extensive application [22–24]. Massive research on polyvinylidene fluoride (PVDF) or its copolymer as separator is ongoing to address aforementioned issues, owing to its superior thermal stability and favorable wettability attributed to the strong electron-absorbing functional groups and low degree of crystallinity [22,25-28]. Nonetheless, their further development is limited in two aspects: (1) short circuit caused by the low mechanical strength of PVDF-based separator associated with Li dendrites and robust electrode; and (2) rapid decay of the discharge capacity resulted from the high activity of Li anode [29,30]. The stable operation of LMBs is still challenged with the unsatisfactory rate performance and heatproof [31–33], low mechanical strength of PVDF-based separators in LMBs [28,34]. To break through these bottlenecks, massive strategies have been used to enhance the overall performances of PVDF-based separators [35]. Recently, it has been demonstrated that polymeric separators incorporated with inor-

* Corresponding author.
E-mail address: weidong.he@hit.edu.cn (W. He).

https://doi.org/10.1016/j.cclet.2021.12.079
1001-8417/

ganic particles (ZrO_2 [36], SiO_2 [37], Al_2O_3 [38] and TiO_2 [39]) or modified with inorganic particles *via* wet method exhibit enhanced electrolyte uptake, mechanical strength and thermal stability. However, the electrolyte shows poor compatibility with the doped inorganic molecules and cells assembled with these composite separators exhibit poor rate performance, severe safety problems and low discharge specific capacity [10,28]. Talcum is a type of layered silicate which is used as reinforcement material for plenty of plastics, owing to its heat-resistance, acid-resistance and insulation. Polymer incorporated with talcum shows excellent rigidity, creep-resistance and stability even at high temperature compared with those incorporated with calcium carbonate or magnesium hydrate [40–42]. On one hand, layered silicate has been demonstrated owning strong interaction and showing superior compatibility with the electrolyte [8,22]. Therefore, compared with inorganic particles (ZrO_2, SiO_2, Al_2O_3, and TiO_2), talcum doped composite separator can improve mechanical properties without sacrificing its rate performance and safety. On the other hand, the layered structure of talcum leads to the parallel ion channels that unify the direction of Li^+ flows. Thus, talcum doped composite separator could improve the discharge specific capacity compared with separators doped with other inorganic particles. Talcum is widely used in composite polymers to reinforce the thermal stability and mechanical strength, reducing the cost at the same time [43].

In our work, a high-rate, safe and low-cost half-cell is designed with the $LiFePO_4$ cathode and the composite separator fabricated by doping talcum into PVDF matrix *via* liquid phase method. As compared with PVDF, PVDF/talcum (PVDF/TM) composite separator with 10 wt% talcum (T-10) owns tiny contact angle of 8° with commercial electrolyte while that of the PVDF is 20°. T-10 achieves the mechanical strength of 33 MPa while the PVDF is 15 MPa, and T-10 attains strain of 253% while that of PVDF is 107%. The cell with $LiFePO_4$ cathode and T-10 can reach 91.7 mAh/g in discharge capacity, higher than cell with PVDF separator (56.3 mAh/g) and cell with the PP separator (51.4 mAh/g) at 10 C.

Talcum is a kind of layered silicate ore consisting of SiO_2 and MgO with the ratio of 2:1, which is stable with the electrolyte and the lithium when being doped with PVDF to form the composite separator [37]. The crystal structure and the atomic configuration of talcum are demonstrated in Figs. S1 and S2 (Supporting information). The structural unit layer of talcum powder consists of a magnesium oxygen octahedron sandwiched by two silicon oxygen tetrahedra. After being incorporated into PVDF to form the PVDF/TM composite separator, the parallel interlayers in talcum provide active sites and uniform channels to transfer Li^+ [22], accelerating the transport of lithium ions as demonstrated in Fig. 1a. The T-10 composite separator exhibits a more porous and uniform structure as compared with PVDF as demonstrated in Figs. 1b and f. The SEM images in Fig. 1c typically display the nanosheet structure of talcum, which is clearly observed in the SEM of T-10 composite separator as depictured in Figs. 1f and g. The energy dispersive spectral (EDS) mapping images of Mg and Si in the T-10 composite separator show the uniform distribution of talcum particles as illustrated in Figs. 1d and h. Moreover, the conclusion is further confirmed with the EDS mapping image of O in T-10 composite separator as depictured in Fig. S3 (Supporting information). The original electron image of EDS is depictured in Fig. S4 (Supporting information). The crystallinities of the talcum particles, PVDF and T-10 separators are analyzed *via* XRD as depictured in Fig. 1e. The characteristic peaks at 9.46° and 19.49° come from the (001) and (101) planes of talcum, respectively. The peak at 28.62° is attributed to quartz, which is commonly found in clays [22]. The original peak at 20.42° of PVDF becomes wide and weak after the addition of talcum, demonstrating that the addition of talcum decreases the crystallinity of the PVDF matrix slightly [44,45]. The FTIR spectra of T-10 composite separator and PVDF separator are shown in Fig. 1i, where the peaks at 614 cm^{-1} and 1402 cm^{-1} come from the α phase of PVDF [46,47]. The peaks that are relevant to the stretching vibration of CF_2 groups appear at 485 cm^{-1} and 1181 cm^{-1} [22,28]. The peaks at 3676 cm^{-1} and 670 cm^{-1} of T-10 composite separator are attributed to the presence of talcum particles.

The thermal distribution is determined with forward looking infrared radiometer (FLIR) as demonstrated in Figs. 2a-c. The T-10 and PVDF separators own the structural integrity, demonstrating the expeditious heat transfer during the whole heating process as shown in Figs. 2b and c, showing a higher thermal stability than PP separators (Fig. 2a). Fig. S5 (Supporting information) shows that PVDF/TM composite separators maintain the most structural integrity even after 30 min at 150 °C, while PP experiences severe shrinkage with the temperature increasing. Fig. S6 (Supporting information) demonstrates that after annealing samples at different temperature, the thermal shrinkage of T-10 composite separator is 1.29% at 120 °C and 5.39% at 150 °C, respectively, far superior to those of PVDF and PP separators. Separators with superior mechanical strength can prevent the cell from short circuit, which is vital for the safe operation of LMBs [1,7,48,49]. The mechanical behavior was investigated with strain-stress analysis as demonstrated in Fig. 2d. As the ratio of talcum in PVDF/TM increases, the mechanical strength of PVDF/TM separators upgrades gently but all much higher than PVDF separator. As for the toughness of these separators, PVDF/talcum (PVDF/TM) composite separator with 5 wt% talcum (T-5) owns nearly 400% elongation, four times than that of PVDF, but sharply decreases with the continued addition of talcum. Given comprehensive comparison on mechanical strength and toughness of these composite separators, T-10 composite separator is chosen to be the ideal separator to carry on further investigation and comparison with PVDF and PP separators. Efficient electrolyte absorption is of great significance for transporting Li^+ [10,50-52]. Electrolyte uptake percentages are measured by immersing the three separators in the commercial electrolyte for one hour, respectively. PVDF-based separator demonstrates a much higher electrolyte uptake percentage than PP, and T-10 composite separator owns the highest uptake percentage of 200% while PVDF of 150% and PP of 120% as demonstrated in Fig. 2e.

Thermogravimetric analysis (TGA) was conducted to further explore the heat endurance of T-10, PVDF and PP separators. The above three separators are heated ranging from 25 °C to 800 °C with the rate of 10 °C/min. The TGA curves demonstrate that T-10 composite separator starts to lose weight at 458 °C, while PVDF at 427 °C and PP at 289 °C, respectively (Fig. 2f). Contact angle measurements are conducted on above three separators to investigate the wettability of the separators. The commercial separator PP owns the contact angle of 48° ± 1.05° due to its intrinsic hydrophobicity while PVDF with 20° ± 1.02° as depictured in Figs. 2g and h [53]. The T-10 composite separator owns the smallest contact angle of 8° ± 1.01° due to the intrinsic hydrophilia of PVDF and the strong compatibility of talcum with electrolyte (Fig. 2i) [28]. Column diagram is used to make a striking contrast among the three separators about contact angle (Fig. S7 in Supporting information).

Rate performance of half-cell with $LiFeO_4$ cathode and PP, PVDF and PVDF/TM separators was investigated. The half-cell with $LiFeO_4$ cathode and Li anode (LFP/Li) with T-10, PVDF/talcum composite separator with 20 wt% talcum (T-20), PVDF/talcum (PVDF/TM) composite separator with 30 wt% talcum (T-30), PVDF and PP separators at 0.2 C, 0.5 C, 1 C, 2 C, 5 C and 10 C are demonstrated respectively in Fig. S8 (Supporting information). The cell with T-10 composite separator reaches 91.78 mAh/g at 10 C with the highest discharge specific capacity, far higher than those with T-20, T-30, PP and PVDF separators. To further investigate the op-

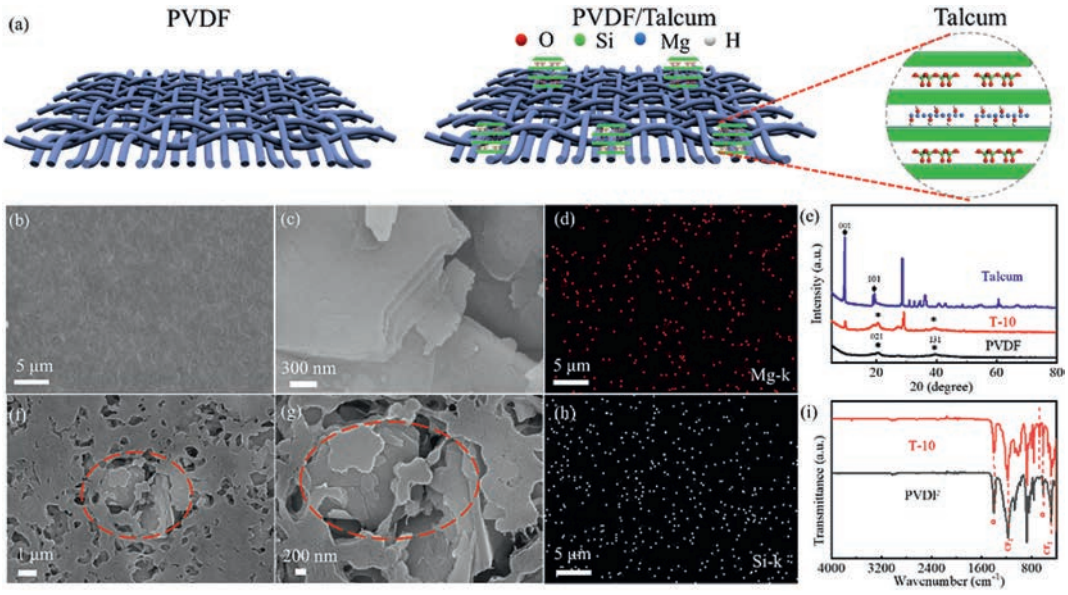

Fig. 1. Fabrication and morphological characteristics of PVDF and T-10 separators. (a) Schematic of PVDF separator, PVDF/TM composite separator and talcum. (b, c) SEM images of PVDF and talcum particle, respectively. (d) Elemental mapping image of Mg-K in a specific acreage of T-10 composite separator. (e) XRD spectra of talcum, PVDF and T-10 separators. (f, g) SEM images of T-10 composite separator at different magnification. (h) Elemental mapping image of Si-K in a specific acreage of T-10 composite separator. (i) FT-IR spectra of T-10 and PVDF separators.

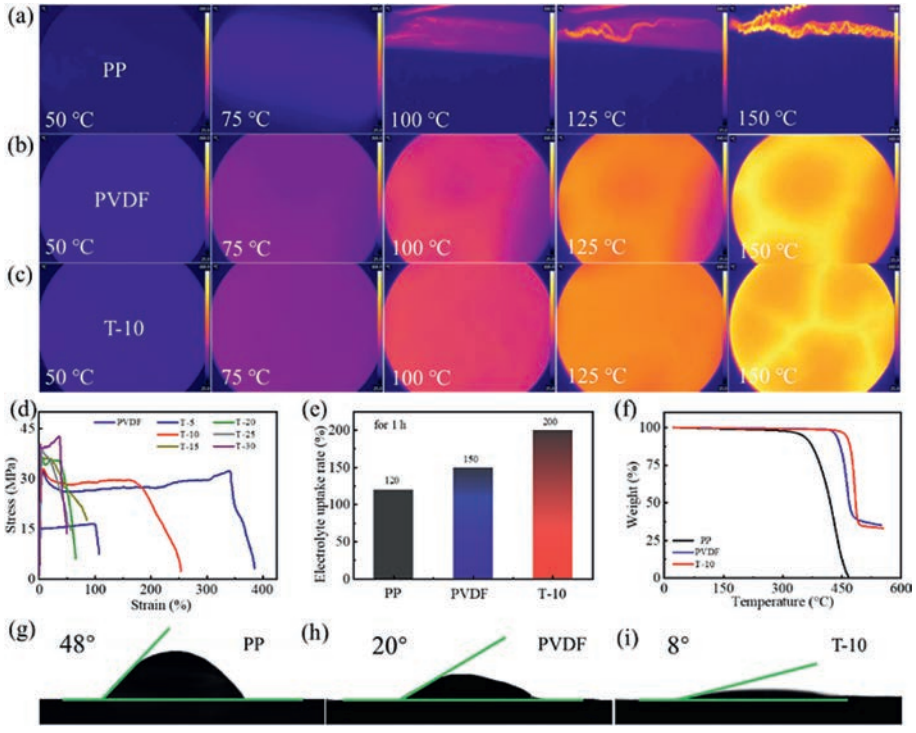

Fig. 2. Heatproof/wettability and other physical performances of PP, PVDF and T-10 separators. (a-c) FLIR pictures of PP, PVDF and the T-10 separators. (d) Tensile curves of PVDF, T-5, T-10, T-15, T-20, T-25 and T-30 separators. (e) Uptake percentage of the PP, PVDF and T-10 separators with commercial electrolyte for 1 h. (f) TG curves of PP, PVDF and T-10 separators. (g-i) Contact angles of PP, PVDF and T-10 separators.

timal proportion of talcum in PVDF, rate performance of the cell with T-5 and PVDF/talcum composite separator with 15 wt% talcum (T-15) composite separators are selected to compare with the cells assembled with T-10 composite separator. As illustrated in Fig. S9 (Supporting information), the cell with T-10 exhibits a discharge specific capacity higher than those with T-5 and T-15 composite separators. The rate properties of the cell assembled with PP, PVDF and T-10 composite separators are selected to make a clear and strong contrast in Fig. 3a. The cell with T-10 reaches discharge capacities of 154.4, 152.3, 149.5, 141.7, 117.7 and 89.8 mAh/g at 0.2 C, 0.5 C, 1 C, 2 C, 5 C and 10 C, respectively. In addition, the discharge specific capacity of the cell with the T-10 recovers to 153.7 mAh/g as 10 C rate returns to 0.2 C, which demonstrates especially stable operation of LFP/Li with T-10 composite separator. On the contrary, cell with both PVDF and PP delivers lower discharge capacity at all rates. The upgraded discharge capacity of the cell assembled with T-10 is attributed to the increased Li^+ channels by adding talcum which is in good agreement with Fig. 1a. However, the rapid dete-

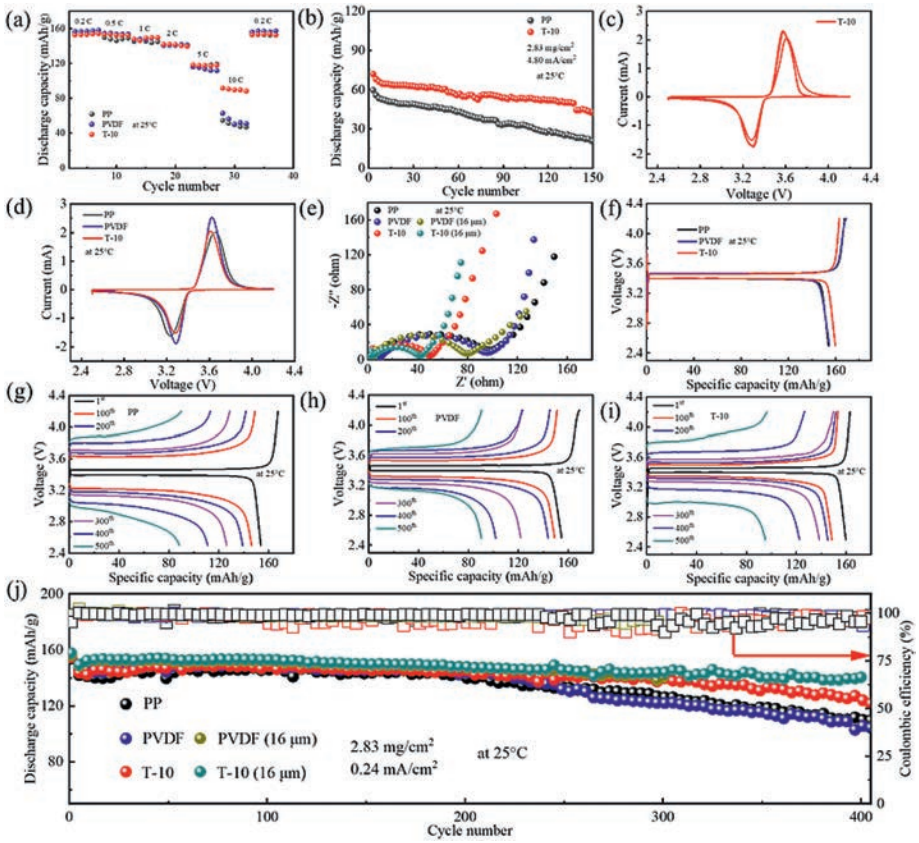

Fig. 3. Electrochemical properties of battery with PP, PVDF and T-10 separators at room temperature. (a) Rate properties of the battery with PP, PVDF and T-10. (b) Cycling properties of the battery with PP and T-10 at 10 C. (c) CV profiles of T-10, recorded with 0.2 mV/s. (d) CV profiles of PP, PVDF and T-10, recorded with 0.2 mV/s. (e) Electrochemical impedance spectroscopy (EIS) curves of the battery with PP, PVDF, T-10, PVDF (16 μm) and T-10 (16 μm) separators. (f) Charging/discharging plots of the cell with PP, PVDF and T-10. (g-i) Charging/discharging plots of the cell with PP, PVDF and T-10, respectively. (j) Cycling properties and Coulombic efficiency of the battery assembled with PP, PVDF, T-10, PVDF (16 μm) and T-10 (16 μm) separators at 0.5 C, respectively.

rioration of discharge capacity happens with excessive talcum particles as a consequence of the long Li^+ transfer path, giving rise to the increased charge transfer resistance as demonstrated in Fig. S10 (Supporting information) [22]. Given this, high-rate cycle-test is conducted on T-10 and PP separators, and discharge capacity of the battery with T-10 composite separator reaches 71.8 mAh/g while that with PP separator reaches 59.5 mAh/g in the first cycle as demonstrated in Fig. 3b. LFP/Li with PVDF/TM separators are put on the working station using the cyclic voltammetry pattern to confirm the electrochemical reactivity, and the peaks at 3.3 V correspond to the reduction and 3.6 V correspond to the oxidation as demonstrated in Fig. 3c, respectively. The solid electrolyte interphase (SEI) is formed during the first cycle of reduction at 3.3 V, and the other two peaks at 3.3 V are attributed to the reduction reactions of the battery. On the contrary, the three sharp peaks at 3.6 V are associated with the oxidization reactions, respectively. The cell with T-10 composite separator shows no obvious fluctuations, demonstrating the especial electrochemical stable of T-10 in half-cell which also can be confirmed in long-cycle property in Fig. 3j. In addition, the CV profiles of cells with PP, PVDF, T-5, T-15, T-20 and T-30 are depictured subsequently in Fig. S11 (Supporting information). The CV curves about the first cycle of PP, PVDF and T-10 are investigated in Fig. 3d, three CV curves show no difference, implying the addition of talcum in PVDF polymeric has no effect on the redox reaction of the cell.

Thickness is a nonnegligible factor of the separator in lithium-based batteries in terms of electrochemical performance and cost [12]. Currently, the thickness of the academic separators is limited to about 25 μm in line with the commercial polyolefin separators. The pursue of thinner separator is becoming urgent for achieving higher energy-density and safer lithium-based batteries [54]. Herein, 16 μm PVDF and 16 μm T-10 separators are fabricated and assembled in the LMBs to investigate the internal resistance and cycle stability as depictured in Figs. 3e and j. To acquire more direct information on the interfacial impendence, the cells with PP, PVDF, T-10, PVDF (16 μm) and T-10 (16 μm) separators are placed on the work station to explore more interface impedance information at open circuit voltage. For cells assembled with PP, PVDF and T-10 separators, minimum semicircle distance is observed in the cell with T-10 composite separator among the three Nyquist curves, demonstrating the lowest transfer impedance, as depictured in Fig. 3e. What is more, cells with 16 μm PVDF and 16 μm T-10 separators show a slight decrease compared with those with 25 μm PVDF and 25 μm T-10 separators as demonstrated in Fig. 3e, respectively. Results show that thin separator can reduce the internal resistance. The cells with separators sandwiched with stainless steel are fabricated to measure the ionic conductivity. The ion conductivity of T-10, PVDF and PP is calculated according to Fig. S12 and Eq. S4 (Supporting information). The ion conductivity of T-10 is 0.509 mS/cm. The symmetrical Li/Li cells with various separators are assembled and tested with 0.5 mA/cm^2 current density to assess the capability of the separator in suppressing the growth of Li dendrites. As demonstrated in Fig. S13 (Supporting information), the cell with T-10 composite separator shows a stable voltage profile over 480 h. In contrast, short circuit occurs on the cells assembled with PP with dramatical voltage fluctuation af-

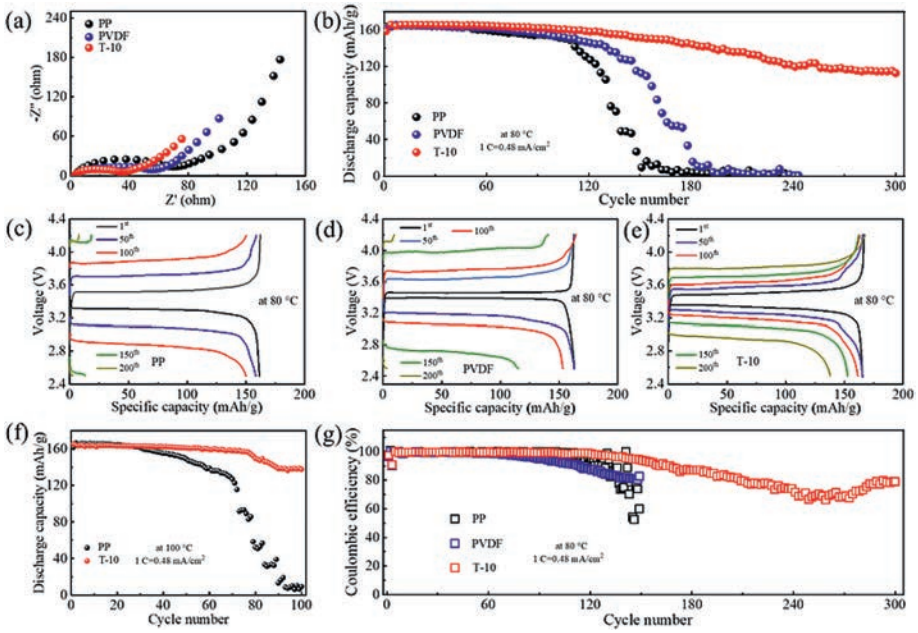

Fig. 4. Electrochemical properties of cell with PP, PVDF and T-10 separators at elevated temperature. (a) EIS curves of the battery assembled with PP, PVDF and T-10 at 80 °C. (b) Cycling properties of cell with PP, PVDF and T-10 at 1 C under 80 °C. (c-e) Charging/discharging plots of cell with PP, PVDF and T-10 at 80 °C. (f) Cycling performance of cell with PP and T-10 at 1 C at 100 °C. (g) Coulombic Efficiency of cell with PP, PVDF and T-10 at 1 C under 80 °C.

ter 300 h. The lithium-ion transference numbers of various separators are illustrated in Fig. S14 (Supporting information). The Li^+ transference number is 0.534 for T-10 separator, which is slightly larger than that of PP (0.509) separators. Fig. 3f illustrates the charge/discharge plots of cell with PP, PVDF and T-10 separators during the same first cycle at 0.5 C, respectively. Results show that the cell with T-10 composite separator owns a discharge specific capacity of 159.78 mAh/g, while PP of 154.67 mAh/g and PVDF of 153.69 mAh/g. The galvanostatic charging/discharging plots of the cell assembled with PP, PVDF and T-10 separators at 0.5 C are depictured in Figs. 3g–i. Cycle stability plays a vital role on the stable operation of the batteries. Cyclic analysis on the cell with PP, PVDF, T-10, PVDF (16 μm) and T-10 (16 μm) separators is conducted at 0.24 mA/cm^2 and the active material loading is 2.83 mg/cm^2, as depictured in Fig. 3j. The battery with T-10 composite separator releases a higher discharge capacity of 122.6 mAh/g, which is maintained at 84% after 400 cycles, while those of the battery with PVDF and PP separators are 73% and 76%, respectively. The cells assembled with PVDF (16 μm) and T-10 (16 μm) separators deliver a slightly higher discharge specific capacity compared with cells with PVDF (25 μm) and T-10 (25 μm) separators. Especially, the cell with T-10 (16 μm) exhibits a capacity that is maintained at 96% after 400 cycles while the cell with PVDF (16 μm) overcharges after 300 cycles, which is depictured in Fig. 3j. LFP/Li half-cells with the T-20 and the T-30 composite separators are also assembled to investigate the cycle stability, which is depictured in Fig. S15 (Supporting information). The linear sweep voltammetry (LSV) is conducted on symmetric Li cells with the T-10 and the PVDF separators. As shown in Fig. S16 (Supporting information), the cell with T-10 and PVDF demonstrated nearly the same voltage sweep up to 4.5 V. In conclusion, the existence of talcum in PVDF has no effect on the electrochemical window.

Aiming to investigate the electrochemical performance of the cell assembled with these separators at high temperature, batteries with $LiFPO_4$ cathode and PP, PVDF and T-10 separators are placed on the work station to explore more interface impedance information with open circuit voltage at 80 °C. The minimum semicircle distance is observed in the cell with T-10 composite separator among the three Nyquist curves, demonstrating the lowest transfer impedance as depictured in Fig. 4a. The semicircle diameters of PP, PVDF and T-10 under 80 °C in Fig. 4a are all smaller than those at room temperature as depictured in Fig. 3e, demonstrating that the rising in temperature can speed up the transfer of lithium ions [55]. The cycle property is conducted on LFP/Li batteries with PP, PVDF and T-10 separators at 80 °C. In Fig. 4b, LFP/Li battery with T-10 separator works extremely stable at 80 °C over 300 cycles, delivering 112.8 mAh/g discharge capacity with 68% retention after 300 cycles. In contrast, LFP/Li battery with PVDF and PP exhibits a sharp decrease in discharge capacity after only 120 cycles. The stable performance of LFP/Li battery with T-10 at elevated temperature is attributed to the excellent thermal stability of talcum, which is confirmed in Fig. 2c and Fig. S5. The coulombic efficiency of the cell with PP, PVDF and T-10 separators is depictured in Fig. 4g, demonstrating that battery with T-10 shows a more stable and higher coulombic efficiency than those with PP and PVDF separators. The galvanostatic charging/discharging plots of the cell with PP, PVDF and T-10 separators at 1 C under 80 °C is verified in Figs. 4c-e. For the initial cycle, the cell with the T-10 separator performs the discharge capacity of 165.92 mAh/g at 1 C under 80 °C, while 161.67 mAh/g and 163.69 mAh/g for PVDF and PP separator as demonstrated in Figs. 4c-e, respectively. The 200th cycle galvanostatic charging/discharging plots of the cell with PP, PVDF and T-10 separators are depictured in Fig. S17 (Supporting information). The temperature is raised to 100 °C to investigate the cycle stability of battery with the T-10 at higher temperature as depictured in Fig. 4f. The battery with T-10 composite separator retains 40 mAh/g after 150 cycles at 100 °C while half-cell with PP shows no discharge capacity after 80 cycles.

The enhanced electrolyte uptake featured with sharply decreased contact angle as confirmed in Figs. 2e and i is associated with the strong interaction between the talcum and the electrolyte. The strong interaction between the talcum and the electrolyte is verified with the DFT simulations as demonstrated in Fig. S18 (Supporting information). The commercial electrolyte is represented by ethylene carbonate (EC), dimethyl ethylene carbonate (DEC) and ethyl methyl carbonate (EMC). The results show

that the adsorption energy values between the talcum and the electrolyte are −1.65 eV for talcum-EMC, −1.70 eV for talcum-EC and −1.64 eV for talcum-DEC, which are much larger than PVDF monomer/electrolyte (−0.02 ∼ −0.08 eV) as demonstrated in Fig. S19 (Supporting information). Owing to the strong affinity to EMC, EC and DEC, the separator doped with talcum shows much more superior electrolyte uptake and wettability when compared with the PP and the PVDF separators. The adsorption energy value of talcum-PVDF monomer (−1.65 eV) as demonstrated in Fig. S20 (Supporting information) is analogous with hydrogen bond strength (−0.01 ∼ −1.68 eV), and much larger than van der Waals forces (−0.004 ∼ −0.04 eV) [56], demonstrating the powerful interaction between the talcum and the PVDF. The optimized model structure of electrolyte through PVDF and T-10 separators are illustrated in Fig. S21 (Supporting information), respectively. The strong interaction between the talcum and the electrolyte contributes to the large amount of electrolyte absorption on the T-10 composite separator. In contrast, only few electrolyte molecule adsorption on the PVDF as depictured in Fig. S21.

In summary, a polymer-based composite separator with high wettability and heat resistance is fabricated by doping the lamellated-clay (talcum) into PVDF. Owing to the strong adsorption energy between the talcum and the electrolyte, the PVDF/TM composite separator owns remarkable electrolyte wettability. The enhanced mechanical strength and toughness of PVDF/TM composite separator are associated with the strong adsorption energy between the talcum and the PVDF monomer and the superior thermal stability of the composite separator is attributed to the heat-proof of talcum. The existence of talcum in PVDF/TM composite separator leads to the parallel ion channels that unify the direction of Li^+ flows, thus improving the discharge specific capacity. Especially, the cell with the T-10 composite separator reaches a remarkable discharge capacity of 91.7 mAh/g while PVDF of 56.3 mAh/g and PP of 51.4 mAh/g at 10 C, owns extremely small contact angle of 8° with commercial electrolyte while PVDF of 20°, achieves the mechanical strength of 33 MPa while PVDF of 15 MPa, and attains strain of 253% while PVDF of 107%, respectively. This work puts forward a novel material to open up the world of the high-rate and safer lithium metal batteries.

Declaration of competing interest

The authors declare that they have no known competing financial interests or personal relationships that could have appeared to influence the work reported in this paper.

Acknowledgments

This research is supported by the Science Foundation of National Key Laboratory of Science and Technology on Advanced Composites in Special Environments, and the National Natural Science Foundation of China (No. 12002109).

Supplementary materials

Supplementary material associated with this article can be found, in the online version, at doi:10.1016/j.cclet.2021.12.079.

References

[1] B.T. Yuan, K.C. Wen, D.J. Chen, et al., Adv. Funct. Mater. 31 (2021) 2101420.
[2] X. Zhang, Q. Sun, C. Zhen, et al., Energy Storage Mater. 37 (2021) 628–647.
[3] L.W. Dong, J.P. Liu, D.J. Chen, et al., ACS Nano 13 (2019) 14172–14181.
[4] J.P. Liu, L.W. Dong, D.J. Chen, et al., Small Methods 4 (2020) 1900753.
[5] C. Zhang, L. Shen, J. Shen, et al., Adv. Mater. 31 (2019) 1808338.
[6] H.Y. Huo, X.N. Li, Y. Chen, et al., Energy Storage Mater. 29 (2020) 361–366.
[7] M.S. Gonzalez, Q.Z. Yan, J. Holoubek, et al., Adv. Mater. 32 (2020) 1906836.
[8] L. Dong, Y. Liu, K. Wen, et al., Adv. Sci. (2021) 2104699.
[9] L. Dong, Y. Liu, D. Chen, et al., Energy Storage Mater. 44 (2022) 527–536.
[10] H. Lee, M. Yanilmaz, O. Toprakci, et al., Energy Environ. Sci. 7 (2014) 3857–3886.
[11] W. Chen, Y. Hu, W.Q. Lv, et al., Nat. Commun. 10 (2019) 4973.
[12] M. Waqas, S. Ali, C. Feng, et al., Small 15 (2019) 1901689.
[13] L.Y. Chou, Y.S. Ye, H.K. Lee, et al., Nano Lett. 21 (2021) 2074–2080.
[14] W.Q. Yao, W.Z. Zheng, J. Xu, et al., ACS Nano 15 (2021) 7114–7130.
[15] X. Li, L.X. Yuan, D.Z. Liu, et al., Adv. Funct. Mater. 31 (2021) 2100537.
[16] P. Chen, Z. Wu, T. Guo, et al., Adv. Mater. 33 (2021) 2007549.
[17] D.J. Chen, C. Feng, Y.P. Han, et al., Energy Environ. Sci. 13 (2020) 2924–2937.
[18] M.F. Lagadec, R. Zahn, V. Wood, Nat. Energy 4 (2019) 16–25.
[19] Y.H. Song, K.J. Wu, T.W. Zhang, et al., Adv. Mater. 31 (2019) 1905711.
[20] C. Zhang, L. Shen, J.Q. Shen, et al., Adv. Mater. 31 (2019) 1808338.
[21] S.Y. Hu, S.D. Lin, Y.Y. Tu, et al., J. Mater. Chem. A 4 (2016) 3513–3526.
[22] J.Y. Zhao, D.J. Chen, B. Boateng, et al., J. Power Sources 451 (2020) 227773.
[23] Y.S. Jung, P. Lu, A.S. Cavanagh, et al., Adv. Energy Mater. 3 (2013) 213–219.
[24] C.J. Orendorff, T.N. Lambert, C.A. Chavez, et al., Adv. Energy Mater. 3 (2013) 314–320.
[25] G.H. Chen, F. Zhang, Z.M. Zhou, et al., Adv. Energy Mater. 8 (2018) 1801219.
[26] H. Li, Y.M. Chen, X.T. Ma, et al., J. Membr. Sci. 379 (2011) 397–402.
[27] M.J. Koh, H.Y. Hwang, D.J. Kim, et al., J. Mater. Sci. Technol. 26 (2010) 633–638.
[28] D.J. Chen, Z.Q. Zhou, C. Feng, et al., Adv. Energy Mater. 9 (2019) 1803627.
[29] A. Gopalan, P. Santhosh, K. Manesh, et al., J. Membr. Sci. 325 (2008) 683–690.
[30] S. Rajendran, Z. Tang, A. George, et al., Adv. Energy Mater. 11 (2021) 2100666.
[31] Q.K. Zhang, X.Q. Zhang, H. Yuan, J.Q. Huang, Small Sci. 1 (2021) 2100058.
[32] W. Cai, C. Yan, Y.X. Yao, et al., Small Struct. 1 (2020) 2000010.
[33] L. Kong, C. Tang, H.J. Peng, et al., SmartMat 1 (2020) e1007.
[34] M.Q. Yang, Y.P. Liu, B.T. Yuan, et al., Mater. Chem. Front. 5 (2021) 2434–2441.
[35] G.D. Kang, Y.M. Cao, J. Membr. Sci. 463 (2014) 145–165.
[36] L. Liu, Y. Wang, C.Y. Gao, et al., J. Membr. Sci. 592 (2019) 117368.
[37] Y. Ma, J.P. Hu, Z.T. Wang, et al., J. Power Sources 451 (2020) 227759.
[38] S. Ali, C. Tan, M. Waqas, et al., Adv. Mater. Interfaces 5 (2018) 1701147.
[39] G.Q. Dong, N.X. Dong, B.X. Liu, et al., J. Membr. Sci. 601 (2020) 117884.
[40] R. Xu, Y.Z. Sun, Y.F. Wang, et al., Chin. Chem. Lett. 28 (2017) 2235–2238.
[41] L. Kong, H.J. Peng, J.Q. Huang, et al., Energy Storage Mater. 8 (2017) 153–160.
[42] H. Dong, P.C. Wang, S.S. Yan, et al., J. Energy Chem. 62 (2021) 423–430.
[43] J. Wiener, H. Kaineder, O. Kolednik, F. Arbeiter, Materials 14 (2021) 725.
[44] M.Y. Li, H.J. Wondergem, M.J. Spijkman, et al., Nat. Mater. 12 (2013) 433–438.
[45] F. Liu, N.A. Hashim, Y. Liu, et al., J. Membr. Sci. 375 (2011) 1–27.
[46] P. Martins, A.C. Lopes, S. Lanceros-Mendez, Prog. Polym. Sci. 39 (2014) 683–706.
[47] X. Cai, T. Lei, D. Sun, L. Lin, RSC Adv. 7 (2017) 15382–15389.
[48] X.B. Cheng, T.Z. Hou, R. Zhang, et al., Adv. Mater. 28 (2016) 2888–2895.
[49] W. Na, A.S. Lee, J.H. Lee, et al., ACS Appl. Mater. Interfaces 8 (2016) 12852–12858.
[50] Q. Zhao, X.T. Liu, S. Stalin, et al., Nat. Energy 4 (2019) 365–373.
[51] J. Liu, Z.N. Bao, Y. Cui, et al., Nat. Energy 4 (2019) 180–186.
[52] Q.J. Wang, Z.X. Jian, W.L. Song, et al., Electrochim. Acta 149 (2014) 176–185.
[53] J.H. Dai, C. Shi, C. Li, et al., Energy Environ. Sci. 9 (2016) 3252–3261.
[54] S. Zhong, B. Yuan, Z. Guang, et al., Energy Storage Mater. 41 (2021) 805–841.
[55] Z.F. Zhou, B.B. Chen, T.T. Fang, et al., Adv. Energy Mater. 10 (2020) 1902023.
[56] Y. Ma, W.S. Tong, W.J. Wang, et al., Compos. Sci. Technol. 168 (2018) 397–403.